Eur. Phys. J. C (2014) 74:3219
DOI 10.1140/epjc/s10052-014-3219-2

THE EUROPEAN PHYSICAL JOURNAL C

Regular Article - Theoretical Physics

Searching for dark matter via mono-Z boson production at the ILC

Wan Neng[1], Song Mao[1,a], Li Gang[1], Ma Wen-Gan[2], Zhang Ren-You[2], Guo Jian-You[1]

[1] School of Physics and Material Science, Anhui University, Hefei 230039, Anhui, People's Republic of China
[2] Department of Modern Physics, University of Science and Technology of China (USTC), Hefei 230026, Anhui, People's Republic of China

Received: 31 March 2014 / Accepted: 8 December 2014 / Published online: 20 December 2014

Abstract High energy colliders provide a new unique way to determine the microscopic properties of dark matter (DM). Weakly interacting massive particles (WIMPs) are widely considered as one of the best DM candidates. It is usually assumed that the WIMP couples to the SM sector through its interactions with quarks and leptons. In this paper, we investigate the DM pair production associated with a Z boson in an effective field theory framework at the international linear collider, which can be used to study the interactions between the DM and leptons. For illustrative purposes, we present the integrated and differential cross sections for the $e^+e^- \to \chi\bar{\chi}Z$ process, where the Z boson is radiated from the initial state electron or positron. Meanwhile, we analyze the neutrino pair production in association with a Z boson as the SM background.

1 Introduction

Observational evidence has confirmed the existence of some kind of cold non-baryonic dark matter (DM), which is the dominant component of matter in our universe [1]. However, astrophysical observations tell us nothing about the mass of the DM particle or whether it interacts with the standard model (SM) particles. In the SM, neutrinos are the only long-lived particles that interact purely via the weak force, but their masses are too small to explain the large mass component in the universe. Thus, to determine the particle nature of DM is one of the most important tasks in cosmology and particle physics.

Among the many DM candidates, weakly interacting massive particles (WIMPs) are the most compelling ones. Primarily this is due to the fact that it offers the possibility to understand the relic abundance of the DM as a natural consequence of the thermal history of the universe [2]. Theories that lie beyond the SM include various extensions of the SM, such as supersymmetry [3–6], universal extra dimensions [7], and little Higgs [8,9], which all naturally lead to good candidates for WIMPs and the cosmological requirements for the WIMP abundance in the universe. In these theoretical frameworks, the WIMP candidates are often both theoretically well motivated and compelling. However, all of these theories still lack experimental support, and we cannot determine the new physics theory to which the DM belongs. Additionally, the first observation of the DM may come from direct or indirect detection experiments, which may not provide information as regards the general properties of the DM particle without offering a way to distinguish between the underlying theories. Thus, model-independent studies of DM phenomenology using effective field theory are particularly important.

Recently, some observational results favor a light DM with a mass around 10 GeV in various experiments. The DAMA experiment has reported a signal of annual modulation at a high significance level [10]. This signal is consistent with the interpretation of the discovery of low mass dark matter in direct measurements by CoGeNT [11], CRESST [12], and CDMS [13] experiments. This region of parameter space is excluded by the other experiments like XENON100 [14], LUX [15], and SuperCDMS [16]. In order to clarify this puzzle, there has been more interesting research in light DM models (where the DM mass is of the order of a few GeV) [17–26]. The high energy colliders are ideal facilities for searching light WIMPs, since they are most effective when producing highly boosted light WIMPs. In the case of a WIMP, stability on the order of the lifetime of the universe implies that pair production must highly dominate over single production, and precludes the WIMP from decaying within the detector volume. WIMPs therefore appear as missing energy, and they can potentially be observed by searching for visible particles recoiling against DM particles [27–34].

The international linear collider (ILC) [35–38] is a proposed positron–electron collider that is planned to operate at

[a] e-mail: songmao@ahu.edu.cn

center of mass energy up to 500 GeV with a potential later upgrade to 1 TeV. Compared with the Large Hadron collider (LHC), the e^+e^- linear collider has a particularly clear background environment. It may have enough energy to produce WIMPs. On the other hand, a positron–electron collider can play a major role in providing precision data for understanding the DM. At the ILC, the DM signal has been studied by directly detecting boson transverse energy signal, such as a mono-photon signal [39–41]. Recently, detection of the DM with a Z boson at the LHC [42,43] has been studied. In this paper, we investigate the DM pair production associated with a Z boson at the ILC.

The paper is arranged as follows: In Sect. 2 we briefly describe the related effective field theory and present the calculation strategy. In Sect. 3, we present some numerical results and discussion. Finally, a short summary is given in Sect. 4.

2 Effective field theory and calculation

We assume that the dark matter candidate is the only new particle which is a singlet under the SM local symmetries, and all SM particles are singlets under the dark-sector symmetries. The interactions between the SM and DM sectors are presumably effected by the exchange of some heavy mediators whose nature we do not need to specify, but we only assume that they are much heavier than the typical scales. Given the assumption that the WIMPs are SM singlets, the factor in each operator consisting of SM fields must also be invariant under SM gauge transformations. The interactions between the DM and SM leptons are described by an effective Lagrangian in Refs. [28–31,44–49]. We do not consider terms with derivatives acting on the leptons, which lead to higher dimensional operators, more suppressed at low energies. The scalar or pseudo-scalar interactions are also suppressed seriously since the strengths of these couplings are proportional to the mass of leptons. The prominent considered coupling feature is in

$$\mathcal{L} = \sum_{\ell} \left\{ \frac{1}{\Lambda_{\rm D5}^2} \bar{\ell}\gamma^{\mu}\ell\bar{\chi}\gamma_{\mu}\chi + \frac{1}{\Lambda_{\rm D8}^2} \bar{\ell}\gamma^{\mu}\gamma^5\ell\bar{\chi}\gamma_{\mu}\gamma^5\chi + \frac{1}{\Lambda_{\rm D9}^2} \bar{\ell}\sigma^{\mu\nu}\ell\bar{\chi}\sigma_{\mu\nu}\chi \right\}, \tag{1}$$

where χ is the DM particle, assumed to be a Dirac fermion, ℓ represents a lepton, and the effective scales $\Lambda_{\rm D5}$, $\Lambda_{\rm D8}$, and $\Lambda_{\rm D9}$ parameterize the vector (D5), axial-vector (D8), and tensor (D9) interactions between the two sectors, respectively. The representative interactions which we consider are mentioned in Ref. [46]. We will typically consider one type of interaction to dominate at a time, and we will thus keep one Λ scale finite while the rest are set to infinity and decoupled.

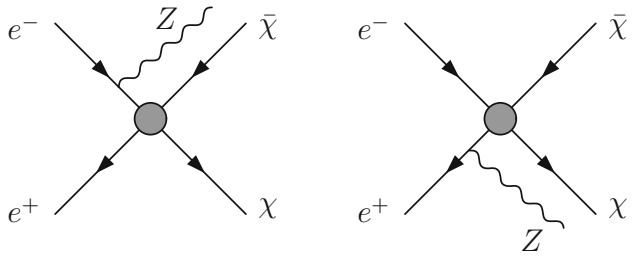

Fig. 1 Tree-level Feynman diagrams for the $e^+e^- \to \chi\bar{\chi}Z$ process

There are two Feynman diagrams contributing to the $e^+e^- \to \chi\bar{\chi}Z$ process at the leading order (LO), shown in Fig. 1.

The amplitudes for the two diagrams are given by

$$\begin{aligned}
\mathcal{M}_{i1} &= \frac{1}{\Lambda_i^2}\bar{u}(p_4)\Gamma_i v(p_3)\bar{v}(p_2)\Gamma^i \frac{i}{\not{p}_1 - \not{p}_5 - m_e} \\
&\quad \times \frac{ie\gamma^{\mu}}{4\sin\theta_W\cos\theta_W}(1-4\sin^2\theta_W-\gamma^5)u(p_1)\epsilon_{\mu}^*(p_5), \\
\mathcal{M}_{i2} &= \frac{1}{\Lambda_i^2}\bar{u}(p_4)\Gamma_i v(p_3)\bar{v}(p_2)\frac{ie\gamma^{\mu}}{4\sin\theta_W\cos\theta_W} \\
&\quad \times (1-4\sin^2\theta_W-\gamma^5)\frac{i}{\not{p}_5-\not{p}_2-m_e}\Gamma_i u(p_1)\epsilon_{\mu}^*(p_5),
\end{aligned} \tag{2}$$

where $\Lambda_i = \Lambda_{D5}$, Λ_{D8}, Λ_{D9}, and $\Gamma_i = \gamma_{\mu}$, $\gamma_{\mu}\gamma_5$, $\sigma_{\mu\nu}$ for vector, axial-vector, and tensor interactions, respectively. p_i $(i = 1,\ldots,5)$ are the four-momenta of the incoming electron, positron, and the outgoing dark matter pair and Z boson, respectively. The differential cross section for the $e^+e^- \to \chi\bar{\chi}Z$ process at tree level is then obtained as

$$\mathrm{d}\sigma_{\rm tree} = \frac{1}{4}\frac{(2\pi)^4}{2s}\sum_{\rm spin}|\mathcal{M}_{\rm tree}|^2\mathrm{d}\Phi_3, \tag{3}$$

where $\mathcal{M}_{\rm tree} = \mathcal{M}_{i1} + \mathcal{M}_{i2}$ is the amplitude of all the tree-level diagrams shown in Fig. 1. The matrix elements $|\mathcal{M}_{\rm tree}|^2$ are listed in the appendix for the vector (D5), axial-vector (D8), and tensor (D9) operators, respectively. The factor $\frac{1}{4}$ is due to taking the average over the spins of the initial particles. $d\Phi_3$ is the three-particle phase space element defined as

$$\mathrm{d}\Phi_3 = \delta^{(4)}\left(p_1 + p_2 - \sum_{i=3}^{5} p_i\right)\prod_{j=3}^{5}\frac{\mathrm{d}^3\vec{p}_j}{(2\pi)^3 2E_j}. \tag{4}$$

In our calculations we adopt the 't Hooft–Feynman gauge. The FeynArts3.4 package [50] is used to generate the Feynman diagrams and convert them into the corresponding amplitudes. The amplitude reductions are mainly implemented by employing FormCalc5.4 package [51].

3 Numerical results and discussion

In this section we present the numerical results for the $e^+e^- \to \chi\bar{\chi}Z$ process at the ILC. The input parameters are taken as [52]

$$\alpha^{-1} = 137.036, \quad m_Z = 91.1876\ \text{GeV}, \\ m_W = 80.385\ \text{GeV}, \quad m_e = 0.511\ \text{MeV}. \tag{5}$$

By using the masses of W and Z bosons, we can obtain the value of the Weinberg mixing angle $\sin^2\theta_W = 1 - \frac{m_W^2}{m_Z^2} = 0.222897$. We have the branch ratio (BR) of Z boson decay to charged leptons ($\text{BR}(Z \to \ell^+\ell^-) = 6.729\,\%$) and hadrons ($\text{BR}(Z \to q\bar{q}) = 69.91\,\%$).

For the $e^+e^- \to \chi\bar{\chi}Z$ process, the final produced particles χ and $\bar{\chi}$ are the missing energy, which will escape the detector without being detected, and the Z boson can be efficiently identified by its leptonic decay. The SM background mainly comes from the $e^+e^- \to \nu\bar{\nu}Z$, $(Z \to \ell^+\ell^-,\ \ell = e, \mu)$ processes, where the neutrino is also the missing energy. Bhabha scattering of leptons with an additional Z boson, $e^+e^- \to e^+e^-Z$, is an important background, which has a large cross section but a very small selection efficiency, since both final state leptons must be undetected. For simplicity of the analysis, we do not consider the background contribution of this part. There are two other important backgrounds, which are $e^+e^- \to W^+W^-$ and $W^\pm l^\mp\nu$ production when the W boson(s) decays leptonically. By adopting appropriate event selection, these backgrounds can also be safely ignored [53]. In Table 1, we list the cross sections of signal and various SM background after different selection cuts.

Cut 1.—select the events containing two opposite sign same-flavor (OSSF) electrons or muons with $p_T > 10$ GeV and $|\eta| < 3$.

Cut 2.—select the events with $\not{E}_T > 30$ GeV.

Cut 3.—select the events where the invariant mass of the two leptons $m_{\ell\ell}$ satisfying $|m_{\ell\ell} - m_Z| < 5$ GeV.

Cut 4.—select the events with $10^o < \theta_{\ell\ell} < 170°$ (where $\theta_{\ell\ell}$ is defined as the zenith angle of the momentum sum of the two leptons).

After these cuts, the signal and main background $e^+e^- \to \nu\bar{\nu}Z$ have very small changes, but the backgrounds, $e^+e^- \to W^+W^-$ and $W^\pm l^\mp\nu$ are suppressed seriously. For the leptonic decay channel, we will mainly study the signal and main SM background $e^+e^- \to \nu\bar{\nu}Z$ in this paper.

In Fig. 2, we present the cross sections as functions of the colliding energy $\sqrt{s}$ for the signal induced by the vector, axial-vector, tensor operators, and the background, including three generations of neutrinos by taking $m_\chi = 10$ GeV and $\Lambda = 1$ TeV with $10° < \theta_z < 170°$ (there θ_z is the angle between the Z boson and the incoming electron beam), respectively. The angular cut can help reducing the background, which contains three flavors of neutrinos. The $\nu_\mu\bar{\nu}_\mu Z$ and $\nu_\tau\bar{\nu}_\tau Z$ production mainly comes from ZZ production and decreases with $\sqrt{s}$, while $\nu_e\bar{\nu}_e Z$ can also come from the t-channel W-exchange diagrams and so increases with $\sqrt{s}$. The ZZ production is rather back-to-back, while the $\chi\bar{\chi}Z$ is less back-to-back, and that is why we imposed a cut on the angle of the Z boson, which will not hurt the signal too much. Moreover, a cut on the scattering angle of Z can avoid radiative return events where a hard photon or a pair of low mass e^+e^- is emitted along the beam direction. From this figure we can see that, with the increment of the colliding energy $\sqrt{s}$, the cross sections for the signal process $e^+e^- \to \chi\bar{\chi}Z$ induced by the vector, axial-vector, and tensor operators increase rapidly, the cross sections for the background from $\nu_e\bar{\nu}_e Z$ production vary slowly, while those backgrounds from $\nu_\mu\bar{\nu}_\mu Z$ and $\nu_\tau\bar{\nu}_\tau Z$ production processes decrease slightly. With the increment of $\sqrt{s}$, the ratio of background to signal declines gradually and the signal becomes significant relative to the background. Con-

Table 1 The cross sections of the signal and SM backgrounds after each cut in the charged leptonic channel at $\sqrt{s} = 500$ GeV are shown, where the DM mass and the scale Λ are taken as $m_\chi = 10$ GeV and $\Lambda = 1$ TeV

	D5	D8	D9	$\nu\bar{\nu}Z$	W^+W^-	$W^\pm l^\mp\nu$
Cut 1	0.158	0.157	1.372	28.07	69.55	92.12
Cut 2	0.135	0.134	1.359	23.74	67.33	78.01
Cut 3	0.135	0.134	1.359	23.75	1.074	4.094
Cut 4	0.135	0.134	1.357	22.92	0.987	3.904

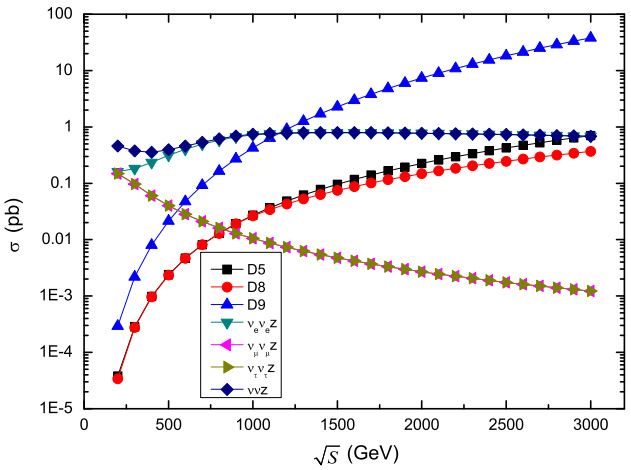

Fig. 2 Total cross sections for the signal process $e^+e^- \to \chi\bar{\chi}Z$ induced by the vector (D5), axial-vector (D8), tensor (D9) operators, and the background processes $e^+e^- \to \nu_\ell\bar{\nu}_\ell Z$ $(\ell = e, \mu, \tau)$ as functions of the colliding energy $\sqrt{s}$ by taking $m_\chi = 10$ GeV, $\Lambda = 1$ TeV and $10° < \theta_z < 170°$

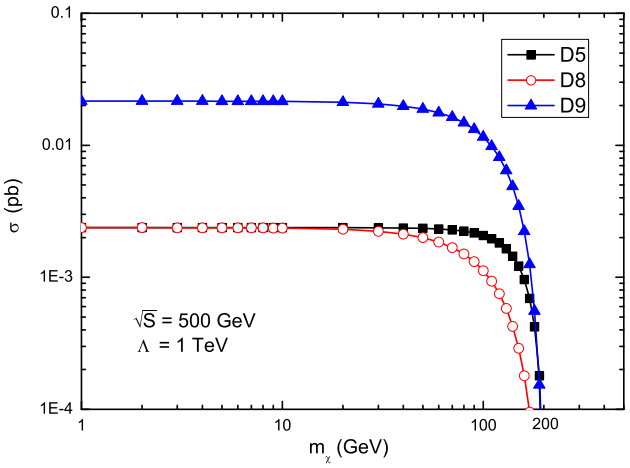

Fig. 3 Dependence of cross sections for the signal process $e^+e^- \to \chi\bar{\chi}Z$ induced by the vector (D5), axial-vector (D8), and tensor (D9) operators on the DM mass with $\sqrt{s} = 500$ GeV, $\Lambda = 1$ TeV, and $10^\circ < \theta_z < 170^\circ$

sequently, we can obtain a larger cross section for the signal and improve the probability for searching DM by increasing the colliding energy $\sqrt{s}$. It should be noted that, for a weak coupling underlying theory, the EFT scale is comparable to the mass scale of the particles which is integrated out. Therefore, the EFT calculations will break down if the center of mass energy involved is much higher than Λ, i.e., $\sqrt{S} > \Lambda$. In order to make the convention unified and convenient, we assume the Λ to be 1 TeV, which does not affect the correctness of the results for $\sqrt{S} > 1$ TeV. Since the cross section for the signal is proportional to $1/\Lambda^4$, we can easily translate the cross section into another one for higher Λ when the center of mass energy $\sqrt{S}$ up to 1 TeV.

In Fig. 3, we present the DM mass dependence of the cross sections for the $e^+e^- \to \chi\bar{\chi}Z$ process induced by the vector, axial-vector, and tensor operators by taking $\sqrt{s} = 500$ GeV, $\Lambda = 1$ TeV, and $10^\circ < \theta_z < 170^\circ$, separately. As shown in this figure, the cross section is insensitive to the DM mass m_χ in the range of $m_\chi < 100$ GeV, and decreases rapidly with the increment of m_χ when $m_\chi > 100$ GeV, which is due to the rapidly reduced phase space. We find that the contributions from the spin-independent operator (D5) and spin-dependent operator (D8) cannot be distinguished until $m_\chi > 100$ GeV.

The significance of the signal over background S is defined as

$$S = \frac{N_S}{\sqrt{N_B}} = \frac{\sigma_S\sqrt{\mathcal{L}}}{\sqrt{\sigma_B}}, \tag{6}$$

where $N_{S,B}$ and $\sigma_{S,B}$ are the event numbers and cross sections for signal and background, and $\mathcal{L}$ denotes the integrated luminosity. In Fig. 4, we depict the 3σ detection region (defined as $S \geq 3$) on the m_χ–Λ plane by taking $\sqrt{s} = 250, 500,$ and 1,000 GeV, $\mathcal{L} = 100$, and 1,000 fb^{-1} after Cut 4, respectively. As mentioned in Fig. 2, we know that Λ has a larger space of adjustment by improving colliding energy. Of course, we can also reach the same effectiveness with the improvement of integrated luminosity. As shown Fig. 4, we can see that Λ will increase with the improvement of $\sqrt{s}$ or integrated luminosity, which is very useful for searching DM. In Table 2, we list the cross sections for the signal process $e^+e^- \to \chi\bar{\chi}Z(Z \to \ell^+\ell^-)$ and the main SM background at the $\sqrt{s} = 250,\ 500,\ 1{,}000$ GeV ILC, and the corresponding significances with $\mathcal{L} = 100$ and 1,000 fb^{-1}, where the DM mass m_χ and the energy scale Λ are taken as 10 GeV and 1 TeV, respectively. Since the cross section for the signal is proportional to $1/\Lambda^4$, we can transform the function of the cross section into a limit on the parameter Λ as shown in Fig. 4. As a side note, the Cut 2 cases are different for the different colliding energy, which are applied, $\not{E}_T > 15$ GeV, $\not{E}_T > 30$ GeV, and $\not{E}_T > 40$ GeV, for $\sqrt{s} = 250$, 500, and 1,000 GeV, respectively.

Polarized beams are sensitive to the chirality of the underlying interactions. One of the major advantages of having an e^+e^- linear collider is the possibility of using polarized beams, which often help in reducing the SM backgrounds and significantly enhance the signal rates [54]. Since new physics signal rates are typically predicted to be very small, making use of polarized beams can offer unique opportunities to discover them. In the baseline design of the ILC [55], the electron (positron) source would be capable to provide a polarized beam with a polarization degree of 80% (30%). With longitudinal polarized beams, the cross section of a process at an e^+e^- collider can be expressed as [54]

$$\begin{aligned}\sigma(P_{e^-}, P_{e^+}) = \frac{1}{4}\big[&(1+P_{e^-})(1+P_{e^+})\sigma_{RR} \\ &+ (1-P_{e^-})(1-P_{e^+})\sigma_{LL} \\ &+ (1+P_{e^-})(1-P_{e^+})\sigma_{RL} \\ &+ (1-P_{e^-})(1+P_{e^+})\sigma_{LR}\big],\end{aligned} \tag{7}$$

where P_{e^-} (P_{e^+}) is the polarization degree of the electron (positron) beam. The right-handed (left-handed) polarization corresponds to $P_{e^\pm} > 0$ ($P_{e^\pm} < 0$). The cross section for the completely left-handed polarized e^- beam ($P_{e^-} = -1$) and completely right-handed polarized e^+ beam ($P_{e^+} = +1$) is denoted σ_{LR}. Besides, σ_{LL}, σ_{RR}, and σ_{RL} have analogous definitions. In this section, we will demonstrate how polarized beams benefit DM searches. We take the case of $\sqrt{s} = 500$ GeV as an illuminating example. In Table 3, we list the unpolarized and polarized results for signal and main background for the charged leptonic channel. We can see that the signals have little difference for the unpolarized and polarized cases, but the SM background is reduced seriously. In Table 4, we investigate the signal significances with unpolarized beams (S_{unpol}) and optimal polarized beams (S_{pol})

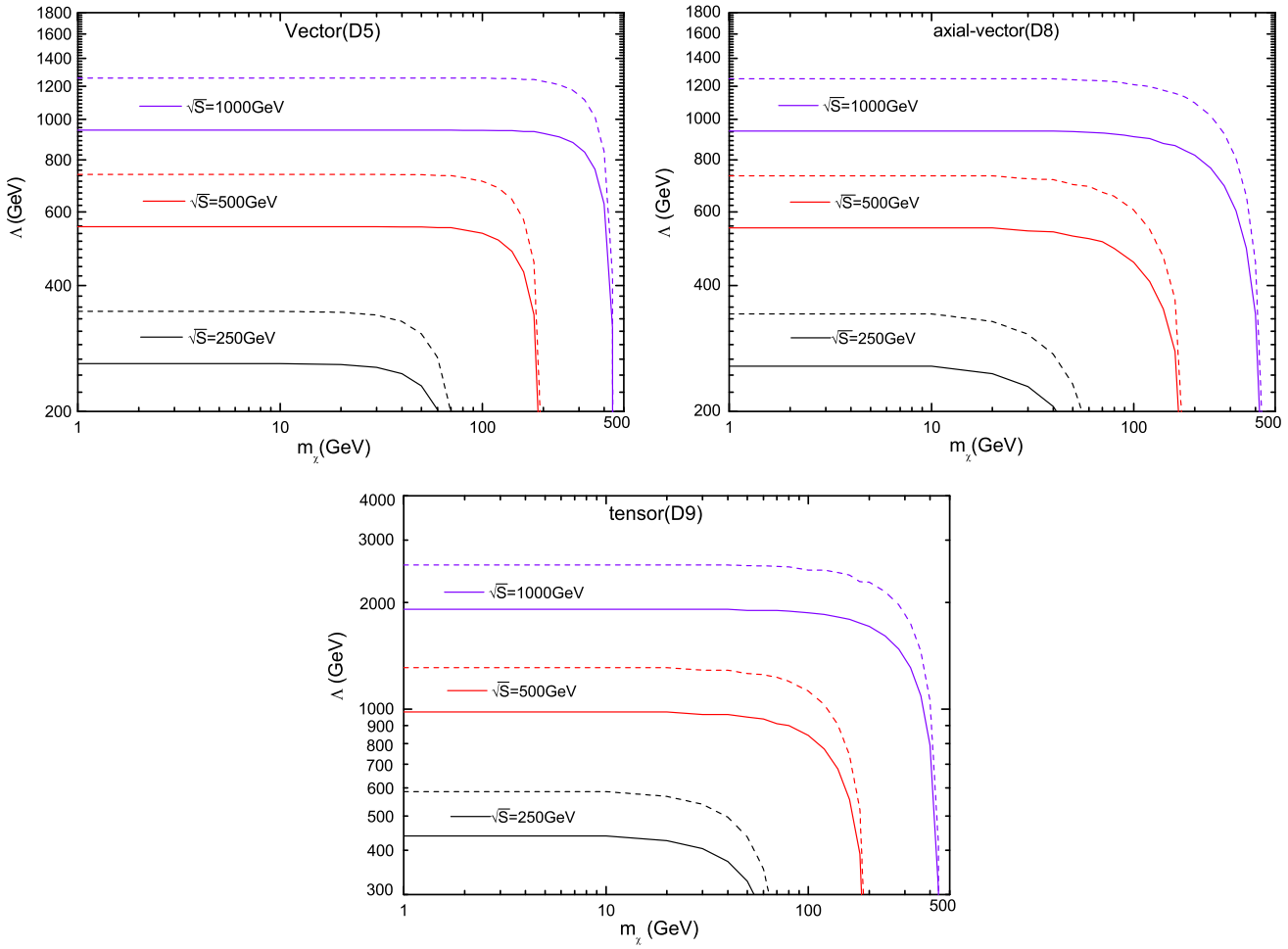

Fig. 4 3σ detection region on the m_χ–Λ plane for the $\chi\bar{\chi}Z(Z \to \ell^+\ell^-)$ production induced by the vector (D5), axial-vector (D8), and tensor (D9) operators at the $\sqrt{s} = 500$ and 1,000 GeV ILC with integrated luminosities of 100 fb^{-1} (*solid lines*) and 1,000 fb^{-1} (*dashed lines*), respectively

Table 2 Cross sections for the signal process $e^+e^- \to \chi\bar{\chi}Z(Z \to \ell^+\ell^-)$ and the main SM background $e^+e^- \to \nu\bar{\nu}Z(Z \to \ell^+\ell^-)$, and the corresponding significances, at the $\sqrt{s} = 250,\ 500,\ 1{,}000$ GeV ILC with $m_\chi = 10$ GeV, $\Lambda = 1$ TeV, and two typical luminosity values of $\mathcal{L}_1 = 100\ \text{fb}^{-1}$ and $\mathcal{L}_2 = 1{,}000\ \text{fb}^{-1}$ after Cut 4

$\sqrt{s}$ (TeV)		σ_S (fb)	σ_B (fb)	$\sigma_S\sqrt{\mathcal{L}_1}/\sqrt{\sigma_B}$	$\sigma_S\sqrt{\mathcal{L}_2}/\sqrt{B}$
0.25	D5	7.19×10^{-3}	27.36	0.0137	0.0435
	D8	6.82×10^{-3}		0.0131	0.0412
	D9	5.81×10^{-2}		0.1111	0.3513
0.5	D5	0.135	22.88	0.2822	0.8925
	D8	0.134		0.2794	0.8264
	D9	1.357		2.8352	8.9712
1.0	D5	1.548	42.98	2.3612	7.4669
	D8	1.546		2.3582	7.4572
	D9	26.87		40.986	129.61

and the ratio $S_{\text{pol}}/S_{\text{unpol}}$. We find that the optimal polarized beams are very helpful to enhance the significance and discover new physics.

In a hadron collider like the LHC, the decay mode $Z \to q\bar{q}$ is harder to control than the mode $Z \to l^+l^-$, since the background involves a huge amount of hadronic jets. While at the ILC the searches may be better performed using the hadronic channel, since the BR of the Z boson decaying to quarks is much larger than decaying to leptons. Therefore, it is important to study the $Z \to q\bar{q}$ decay mode as well with its associated backgrounds, and make a comparison with the leptonic mode.

Similar to the charged leptonic decay channel, we list the unpolarized and polarized results for signal and main SM background for the hadronic channel in Table 5. In Table 6, we investigate the signal significances with unpolarized

Table 3 Cross sections (in fb) of the signals and main background under various polarization configurations after applying selection cuts are demonstrated for the charge leptonic channel at $\sqrt{s} = 500$ GeV, where the DM mass and the scale Λ are taken as $m_\chi = 10$ GeV and $\Lambda = 1$ TeV

(P_{e^-}, P_{e^+})	D5	D8	D9	$\nu\bar{\nu}Z(Z \to \ell^+\ell^-)$
(0, 0)	0.135	0.134	1.357	22.92
(+0.8, −0.3)	0.135	0.134	1.031	7.925
(+0.8, +0.3)	0.088	0.087	1.683	8.089
(−0.8, −0.3)	0.117	0.116	1.683	26.64
(−0.8, +0.3)	0.199	0.198	1.031	48.74

Table 4 In the optimal polarization configuration (+0.8, −0.3), signal significances with unpolarized beams (S_{unpol}) and with optimal polarized beams (S_{pol}) for the charge leptonic channel at $\sqrt{s} = 500$ GeV are compared with an integrated luminosity $\mathcal{L} = 100\,\text{fb}^{-1}$, where the DM mass and the scale Λ are taken as $m_\chi = 10$ GeV and $\Lambda = 1$ TeV

	$\mathcal{S}_{\text{unpol}}$	$\mathcal{S}_{\text{pol}}$	$\mathcal{S}_{\text{pol}}/\mathcal{S}_{\text{unpol}}$
D5	0.282	0.481	1.705
D8	0.279	0.477	1.710
D9	2.835	3.664	1.292

Table 5 Cross sections (in fb) of the signals and main background under various polarization configurations after applying selection cuts are demonstrated for the hadronic channel at $\sqrt{s} = 500$ GeV, where the DM mass and the scale Λ are taken as $m_\chi = 10$ GeV and $\Lambda = 1$ TeV

(P_{e^-}, P_{e^+})	D5	D8	D9	$\nu\nu Z(Z \to q\bar{q})$
(0, 0)	1.401	1.391	14.10	212.1
(+0.8, −0.3)	1.407	1.397	10.72	62.72
(+0.8, +0.3)	0.915	0.908	17.48	70.15
(−0.8, −0.3)	1.215	1.206	17.48	252.2
(−0.8, +0.3)	2.067	2.052	10.72	463.2

beams (S_{unpol}) and optimal polarized beams (S_{pol}) and the ratio $S_{\text{pol}}/S_{\text{unpol}}$. In Fig. 5, we depict the 3σ detection region (defined as $S \geq 3$) on the m_χ–Λ plane for the hadronic decay channel by taking $\sqrt{s} = 250$, 500, and 1,000 GeV, $\mathcal{L} = 100$, and 1,000 fb^{-1}, respectively. In these parts, we have applied three selection cuts to the final particles.

Cut 1.—Select the events containing two jets with $p_T > 10$ GeV and $|\eta| < 3$.

Cut 2.—Select the events with $\not{E}_T > 30$ GeV.

Cut 3.—Select the events with $10^\circ < \theta_{jj} < 170^\circ$.

Compared with the leptonic mode, we find that there are more events for the hadronic channel, and the signal significance is also more notable.

The mono-photon and missing energy signature has been widely studied in the context of the LEP experiment and

Table 6 In the optimal polarization configuration (+0.8, −0.3), signal significances with unpolarized beams (S_{unpol}) and with optimal polarized beams (S_{pol}) for the hadronic channel at $\sqrt{s} = 500$ GeV are compared with an integrated luminosity $\mathcal{L} = 100\,\text{fb}^{-1}$, where the DM mass and the scale Λ are taken as $m_\chi = 10$ GeV and $\Lambda = 1$ TeV

	$\mathcal{S}_{\text{unpol}}$	$\mathcal{S}_{\text{pol}}$	$\mathcal{S}_{\text{pol}}/\mathcal{S}_{\text{unpol}}$
D5	0.962	1.776	1.846
D8	0.955	1.763	1.846
D9	9.683	13.53	1.397

is well known to provide bounds on the operators considered by the authors of Ref. [39,40]. It is interesting to compare our results with those estimated in Ref. [40], where the authors considered the DM production associating with an initial state radiated photon, $e^+e^- \to \chi\bar{\chi}\gamma$. We find that our results are much less sensitive, especially at $\sqrt{s} = 250$ GeV, because the initial state radiated Z boson is massive and suppresses the phase space of the DM production cross section. When the collision energy increases to 1 TeV, the Z boson mass becomes negligible and the cross sections of these two processes are roughly equal at such a high energy. The bound on Λ is lower than that in Ref. [40] in high energy; this is due to the small BR of the Z boson. After considering the total contribution of the charged leptonic and hadronic decay channel, one will have less difference between these two processes. Therefore, the mono-Z production process is an important channel to search DM and SM particle interactions as well as mono-photon production.

Previous studies of direct and indirect measurements have begun to constrain the physical properties of dark matter. If the WIMP–quark operator mediates spin-independent WIMP–nucleon scattering at low velocities, such as scalar or vector operators, the bounds from direct detection are very strong. The current XENON100 bound [14] rules out these kinds of operators up to $\Lambda \sim 20$ TeV [40]. If the WIMP–quark operator only mediates spin-dependent WIMP–nucleon scattering (e.g. we have axial-vector or tensor couplings), then the direct detection bounds on Λ are weaker, of the order of a few hundred GeV. The lack of any significant gamma-ray excess in the Fermi Large Area Telescope leads to the exclusion of generic dark matter candidates with annihilation cross sections on the order of the benchmark value for a thermal relic ($3 \times 10^{-26}\,\text{cm}^3\,\text{s}^{-1}$) and with masses less than a few tens of GeV. Despite the constraints being very strong as seen from the current detections, which become limited for WIMP masses below 10 GeV, the collider searches can provide a sensitive probe in that region. Especially, for many operators, the colliders become the only way to effectively probe WIMP and SM particle interactions. The current LHC bounds on Λ are of the order of 700 GeV, which is lower than at ILC for both mono-photon and mono-Z pro-

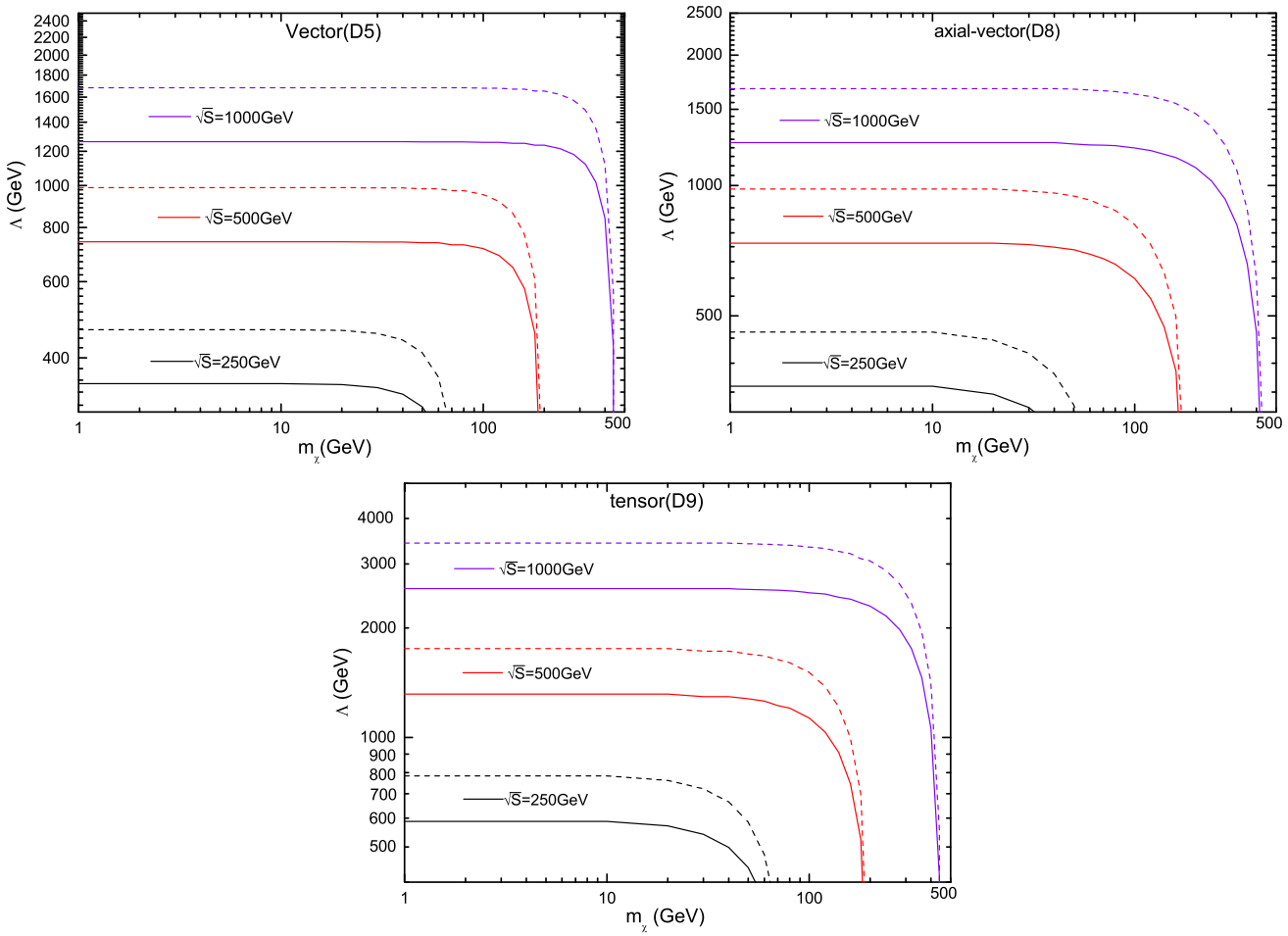

Fig. 5 3σ detection region on the m_χ–Λ plane for the $\chi\bar{\chi}Z(Z \to q\bar{q})$ production induced by the vector (D5), axial-vector (D8), and tensor (D9) operators at the $\sqrt{s} = 500$ and 1,000 GeV ILC with integrated luminosities of 100 fb^{-1} (*solid lines*) and 1,000 fb^{-1} (*dashed lines*), respectively

duction. Therefore, we conclude that ILC searches will be more sensitive to much higher scales.

4 Summary

The origin of dark matter remains one of the most compelling mysteries in our understanding of the universe today. High energy colliders are ideal facilities to search for DM. In this paper, we study the effects of the effective operators of DM via dark matter pair production associated to a Z boson at the ILC. The SM main background $e^+e^- \to \nu\bar{\nu}Z$ is also considered for comparison. For the Z decay to charged lepton and hadron pairs, we apply different selection cuts for the final particles and analyze both the signal and the main background at various colliding energies and luminosities. We obtain the cross sections as functions of colliding energy $\sqrt{s}$ and the DM mass m_χ for the signal induced by the vector, axial-vector, and tensor operators and the SM background. We find that increasing the colliding energy can improve the probability for finding DM, and the contributions from the spin-independent operator (D5) and the spin-dependent operator (D8) cannot be distinguished until $m_\chi > 100$ GeV. If this signal is not observed at the ILC, we set a lower limit on the new physics scale Λ at the 3σ level for both charged leptonic and hadronic channels. We investigate the case of polarized beams for both charged leptonic and hadronic channels, and we find that the optimal polarized beams can enhance the significance and reduce the SM background. We conclude that the ILC has the potential to detect the $e^+e^- \to \chi\bar{\chi}Z$ production.

Acknowledgments This work was supported in part by the National Natural Science Foundation of China (No. 11205003, No. 11305001, No. 11275190, No. 11375171, No. 11175001), the Key Research Foundation of Education Ministry of Anhui Province of China (No. KJ2012A021), the Youth Foundation of Anhui Province (No. 1308085QA07), and financed by the 211 Project of Anhui University (No. 02303319).

Note added While this paper was being reviewed, Ref. [56] appeared which overlaps with our work. Our results agree with the results in Ref. [56] induced by the vector (D5) and axial-vector (D8) interactions.

Appendix

In this appendix, we list the matrix elements $|\mathcal{M}_{tree}|^2$ induced by the vector (D5), axial-vector (D8), and tensor (D9) operators for processes $e^+e^- \to \chi\bar{\chi}Z$, respectively. Due to the mass of electron m_e being very small, we neglect all the terms related to the m_e. The kinematic invariants are defined as $s = (p_1 + p_2)^2, t = (p_1 - p_3)^2, u = (p_2 - p_3)^2$, $s_{34} = (p_3 + p_4)^2$, $t_{14} = (p_1 - p_4)^2$, and $t_{24} = (p_2 - p_4)^2$. Our results read

$$
\begin{aligned}
&|\mathcal{M}_{tree}|^2_{D5} \\
&= \frac{e^2(1-4s_w^2+8s_w^4)}{\Lambda^4 m_Z^2 s_w^2 c_w^2(-2m_\chi^2+s_{34}+t_{24}+u)^2} \\
&\times \{8m_\chi^8+4m_\chi^6(4m_Z^2+2s-2s_{34}-t-t_{14}-3t_{24}-3u) \\
&+ (s_{34}+t_{24}+u)^2(tt_{24}+t_{14}u)+2m_Z^2(s_{34}(t_{14}t_{24}+tu) \\
&- (t_{24}-u)(tt_{24}-t_{14}u)+s(2t_{24}u+s_{34}(t_{24}+u))) \\
&+ 2m_\chi^4(-4ss_{34}+s_{34}^2+2s_{34}t+2s_{34}t_{14}-4st_{24}+4s_{34}t_{24} \\
&+ 4tt_{24}+2t_{14}t_{24}+3t_{24}^2-4su+4s_{34}u+2tu+4t_{14}u \\
&+ 6t_{24}u+3u^2+2m_Z^2(s+s_{34}-2(t+t_{14}+t_{24}+u))) \\
&- m_\chi^2[(s_{34}+t_{24}+u)(5tt_{24}+t_{14}t_{24}+t_{24}^2+tu+5t_{14}u \\
&+ 2t_{24}u+u^2-2s(s_{34}+t_{24}+u)+s_{34}(t+t_{14}+t_{24}+u)) \\
&+ 2m_Z^2(-3tt_{24}-t_{14}t_{24}-t_{24}^2-tu-3t_{14}u+2t_{24}u-u^2 \\
&+ 2s(2s_{34}+t_{24}+u)+s_{34}(t+t_{14}+t_{24}+u))]\},
\end{aligned}
$$

$$
\begin{aligned}
&|\mathcal{M}_{tree}|^2_{D8} \\
&= \frac{e^2(1-4s_w^2+8s_w^4)}{\Lambda^4 m_Z^2 s_w^2 c_w^2(-2m_\chi^2+s_{34}+t_{24}+u)^2} \\
&\times \{8m_\chi^8-4m_\chi^6(4m_Z^2+2s+2s_{34}+t+t_{14}+3t_{24}+3u) \\
&+ (s_{34}+t_{24}+u)^2(tt_{24}+t_{14}u) \\
&+ 2m_Z^2(s_{34}(t_{14}t_{24}+tu)-(t_{24}-u)(tt_{24}-t_{14}u) \\
&+ s(2t_{24}u+s_{34}(t_{24}+u)))+2m_\chi^4(s_{34}^2+2s_{34}t+2s_{34}t_{14} \\
&+ 4s_{34}t_{24}+4tt_{24}+2t_{14}t_{24}+3t_{24}^2+4s_{34}u \\
&+ 2tu+4t_{14}u+6t_{24}u+3u^2+4s(s_{34}+t_{24}+u) \\
&+ 2m_Z^2(s+s_{34}+2(t+t_{14}+t_{24}+u))) \\
&- m_\chi^2[2s(s_{34}^2+2s_{34}(t_{24}+u)+(t_{24}+u)(2m_Z^2+t_{24}+u)) \\
&+ (s_{34}+t_{24}+u)(t_{14}t_{24}+t_{24}^2+5t_{14}u+2t_{24}u+u^2 \\
&+ s_{34}(t+t_{14}+t_{24}+u)+t(5t_{24}+u)) \\
&+ 2m_Z^2(3t_{14}t_{24}-t_{24}^2+t_{14}u+2t_{24}u-u^2 \\
&+ s_{34}(t+t_{14}+t_{24}+u)+t(t_{24}+u)))]\},
\end{aligned}
$$

$$
\begin{aligned}
&|\mathcal{M}_{tree}|^2_{D9} \\
&= \frac{4e^2(1-4s_w^2+8s_w^4)}{\Lambda^4 m_Z^2 s_w^2 c_w^2(-2m_\chi^2-m_Z^2+s+t+t_{14})^2} \\
&\times \{16m_\chi^8-8m_\chi^6(s+3t+3t_{14}+t_{24}+u) \\
&+ 2m_Z^2(s+t+t_{14})(4t_{24}u+s_{34}(t_{24}+u)) \\
&+ m_Z^4(ss_{34}-2(tt_{24}+t_{14}u))-(s+t+t_{14})^2 \\
&\times (ss_{34}-2(tt_{24}+t_{14}u))+4m_\chi^4(-m_Z^4-s^2+3t^2 \\
&+ 6tt_{14}+3t_{14}^2+4tt_{24}+2t_{14}t_{24}+2tu+4t_{14}u \\
&+ 2m_Z^2(s_{34}+t_{24}+u)+s(-s_{34}+2(t+t_{14}+t_{24}+u))) \\
&- 2m_\chi^2[m_Z^4(s-t-t_{14}-t_{24}-u)-(s+t+t_{14}) \\
&\times (s^2-t^2-2tt_{14}-t_{14}^2-5tt_{24}-t_{14}t_{24}+s(2s_{34}-t_{24}-u) \\
&- tu-5t_{14}u)+2m_Z^2(tt_{24}+t_{14}t_{24}+tu+t_{14}u+4t_{24}u \\
&+ s(s_{34}+t_{24}+u)+s_{34}(t+t_{14}+t_{24}+u))]\}.
\end{aligned}
$$

References

1. G. Bertone, D. Hooper, J. Silk, Phys. Rept. **405**, 279 (2005). arXiv:hep-ph/0404175
2. J.L. Feng, J. Kumar, Phys. Rev. Lett. **101**, 231301 (2008). arXiv:0803.4196 [hep-ph]
3. J. Wess, B. Zumino, Nucl. Phys. B C **70**(1), 39–50 (1974)
4. S.P. Martin, In: Kane, G.L. (ed.): Perspectives on Supersymmetry II*, pp. 1–153 arXiv:hep-ph/9709356
5. M. Drees, R. Godbole, P. Roy, Theory and phenomenology of sparticles: an account of four-dimensional $N = 1$ supersymmetry in high energy physics (2004)
6. H.P. Nilles, Phys. Rept. **110**, 1–C162 (1984)
7. T. Appelquist, H.-C. Cheng, B.A. Dobrescu, Phys. Rev. D **64**, 035002 (2001). arXiv:hep-ph/0012100 [hep-ph]
8. N. Arkani-Hamed, A.G. Cohen, H. Georgi, Phys. Lett. B **513**, 232–C240 (2001). arXiv:hep-ph/0105239 [hep-ph]
9. H.-C. Cheng, I. Low, JHEP **0309**, 051 (2003). arXiv:hep-ph/0308199 [hep-ph]
10. R. Bernabei et al., DAMA and LIBRA Collaborations. Eur. Phys. J. C **67**, 39 (2010). arXiv:1002.1028 [astro-ph.GA]
11. CoGeNT Collaboration, C. Aalseth, P. Barbeau, J. Colaresi, J. Collar, J. Diaz Leon, et al. Phys. Rev. Lett. **107**, 141301 (2011). arXiv:1106.0650 [astro-ph]
12. CRESST Collaboration, G. Angloher et al., Eur. Phys. J. C **72**, 1971 (2012). arXiv:1109.0702 [astro-ph]
13. C.D.M.S. Collaboration, R. Agnese et al., Phys. Rev. Lett. **111**, 251301 (2013). arXiv:1304.4279 [hep-ex]
14. XENON100 Collaboration, E. Aprile et al., Phys. Rev. Lett. **109**, 181301 (2012). arXiv:1207.5988
15. L.U.X. Collaboration, D.S. Akerib et al., Phys. Rev. Lett. **112**, 091303 (2014)
16. SuperCDMS Collaboration, R. Agnese et al., Phys. Rev. Lett. **112**, 241302 (2014)
17. Y.G. Kim, S. Shin, JHEP **0905**, 036 (2009). arXiv:0901.2609 [hep-ph]
18. A.L. Fitzpatrick, D. Hooper, K.M. Zurek, Phys. Rev. D **81**, 115005 (2010). arXiv:1003.0014 [hep-ph]
19. J. Kopp, T. Schwetz, J. Zupan, JCAP **1002**, 014 (2010). arXiv:0912.4264 [hep-ph]
20. E. Kuflik, A. Pierce, K.M. Zurek, Phys. Rev. D **81**, 111701 (2010). arXiv:1003.0682 [hep-ph]

21. S. Andreas, C. Arina, T. Hambye, F.-S. Ling, M.H.G. Tytgat, Phys. Rev. D **82**, 043522 (2010). arXiv:1003.2595 [hep-ph]
22. S. Chang, J. Liu, A. Pierce, N. Weiner, I. Yavin, JCAP **1008**, 018 (2010). arXiv:1004.0697 [hep-ph]
23. R. Essig, J. Kaplan, P. Schuster, N. Toro. arXiv:1004.0691 [hep-ph]
24. H. An, S.L. Chen, R.N. Mohapatra, S. Nussinov, Y. Zhang, Phys. Rev. D **82**, 023533 (2010). arXiv:1004.3296 [hep-ph]
25. V. Barger, M. McCaskey, G. Shaughnessy, Phys. Rev. D **82**, 035019 (2010). arXiv:1005.3328 [hep-ph]
26. D. Hooper, J.I. Collar, J. Hall, D. McKinsey, C. Kelso, Phys. Rev. D **82**, 123509 (2010). arXiv:1007.1005 [hep-ph]
27. A. Birkedal, K. Matchev, M. Perelstein, Phys. Rev. D **70**, 077701 (2004). [hep-ph/0403004]
28. M. Beltran, D. Hooper, E.W. Kolb, Z.C. Krusberg, Phys. Rev. D **80**, 043509 (2009). arXiv:0808.3384 [hep-ph]
29. Q.-H. Cao, C.-R. Chen, C.S. Li, H. Zhang, JHEP **1108**, 018 (2011). arXiv:0912.4511 [hep-ph]
30. M. Beltran, D. Hooper, E.W. Kolb, Z.A.C. Krusberg, T.M.P. Tait, JHEP **1009**, 037 (2010). arXiv:1002.4137 [hep-ph]
31. W. Shepherd, T.M.P. Tait, G. Zaharijas, Phys. Rev. D **79**, 055022 (2009). arXiv:0901.2125 [hep-ph]
32. I.F. Ginzburg, PoS QFTHEP **2010**, 028 (2010). arXiv:1010.5579 [hep-ph]
33. I.F. Ginzburg, arXiv:1211.2429 [hep-ph]
34. A. Crivellin, F. D'Eramo, M. Procura, Phys. Rev. Lett. **112**, 191304 (2014). arXiv:1402.1173 [hep-ph]
35. J. Brau, Y. Okada, N.Walker, arXiv:0712.1950 [physics.acc-ph]
36. A. Djouadi et al., arXiv:0709.1893 [hep-ph]
37. N. Phinney, N. Toge, N. Walker, arXiv:0712.2361 [physics.acc-ph]
38. T. Behnke et al., ArXiv e-prints (2007). arXiv:0712.2356 [physics.ins-det]
39. H. Dreiner, M. Huck, M. Kramer, D. Schmeier, J. Tattersall, Phys. Rev. D **87**(7), 075015 (2013). arXiv:1211.2254 [hep-ph]
40. Y.J. Chae, M. Perelstein, JHEP **1305**, 138 (2013). arXiv:1211.4008 [hep-ph]
41. Z.-H. Yu, Q.-S. Yan, P.-F. Yin, arXiv:1307.5740 [hep-ph]
42. L.M. Carpenter, A. Nelson, C. Shimmin, T.M.P. Tait, D. Whiteson, Phys. Rev. D **87**(7), 074005 (2013). [arXiv:1212.3352]
43. N.F. Bell, J.B. Dent, A.J. Galea, T.D. Jacques, L.M. Krauss, T.J. Weiler, Phys. Rev. D **86**, 096011 (2012). arXiv:1209.0231 [hep-ph]
44. J. Goodman, M. Ibe, A. Rajaraman, W. Shepherd, T.M.P. Tait, H.-B. Yu, Phys. Lett. **B695**, 185 (2011). arXiv:1005.1286 [hep-ph]
45. Y. Bai, P.J. Fox, R. Harnik, JHEP **1012**, 048 (2010). arXiv:1005.3797 [hep-ph]
46. J. Goodman, M. Ibe, A. Rajaraman, W. Shepherd, T.M.P. Tait, H.-B. Yu, Phys. Rev. D **82**, 116010 (2010). arXiv:1008.1783 [hep-ph]
47. A. Rajaraman, W. Shepherd, T.M.P. Tait, A.M. Wijangco, Phys. Rev. D **84**, 095013 (2011). arXiv:1108.1196 [hep-ph]
48. P.J. Fox, R. Harnik, J. Kopp, Y. Tsai, Phys. Rev. D **85**, 056011 (2012). arXiv:1109.4398 [hep-ph]
49. K. Cheung, P.-Y. Tseng, Y.-L.S. Tsai, T.-C. Yuan, JCAP **1205**, 001 (2012). arXiv:1201.3402 [hep-ph]
50. T. Hahn, Comput. Phys. Commun. **140**, 418 (2001)
51. T. Hahn, M. Perez-Victoria, Comput. Phys. Commun. **118**, 153 (1999)
52. Particle Data Group Collaboration, K. Nakamura et al., J. Phys. G **37**, 075021 (2010)
53. K.-m. Cheung, W.-Y. Keung, Phys. Rev. D **60**, 112003 (1999). hep-ph/9903294
54. G. Moortgat-Pick, T. Abe, G. Alexander, B. Ananthanarayan, A.A. Babich, V. Bharadwaj, D. Barber, A. Bartl et al., Phys. Rept. **460**, 131 (2008). hep-ph/0507011
55. C. Adolphsen, M. Barone, B. Barish, K. Buesser, P. Burrows, J. Carwardine, J. Clark, H.M. Durand et al., arXiv:1306.6328 [physics.acc-ph]
56. Z.H. Yu, X.J. Bi, Q.S. Yan, P.F. Yin, arXiv:1404.6990 [hep-ph]